Journal of Cluster Science (2022) 33:925–933
https://doi.org/10.1007/s10876-021-02025-4

ORIGINAL PAPER

Facile Green Synthesis of Copper Oxide Nanoparticles and Their Rhodamine-b Dye Adsorption Property

Mohd Yousuf Rather[1] · Somaiah Sundarapandian[1]

Received: 3 October 2020 / Accepted: 5 February 2021 / Published online: 23 February 2021

Abstract

Adsorption has gained more popularity in wastewater treatment because the process is non-toxic, cheap, and highly efficient. Environmental and human-friendly adsorbents specifically have a vast prospective. Hence, in the present study, copper oxide nanoparticles (CuONPs) synthesized with *Wedelia urticifolia* leaf extract were used as adsorbents for Rhodamine-b (RhB) dye. The biomolecules responsible for the synthesis were predicted from Fourier transform infrared (FT-IR) analysis while UV–Visible (UV–Vis) spectroscopy, Dynamic laser spectroscopy (DLS), X-ray diffraction (XRD), and Transmission electron microscopy (TEM) techniques were used for particle characterization. The results revealed that the synthesized nanoparticles are crystalline and spherical with a size of less than 40 nm. The dye adsorption characteristics from the aquatic environment were investigated at room temperature under different doses of CuONPs, initial concentration of RhB dye, and contact time, and over 99% of RhB dye removal was achieved. The adsorption process of RhB dye onto the as-synthesized CuONPs was accurately described by the Freundlich isotherm and pseudo-second-order kinetic models. In summary, the as-synthesized nanoparticles possess an excellent ability for RhB adsorption, and hence these nanoparticles can be used as inexpensive, promising, and potential alternatives to traditional wastewater treatment techniques.

Keywords Adsorption · Dye removal · Leaf extract · Nanoparticles · Wastewater treatment

Introduction

Industrial wastewater contaminated with toxic and hazardous pollutants is one of the grave environmental concerns. Among all these pollutants, dyes are of more significant concern because the color due to dyes is a visible and undesirable property [1]. Dyes constitute a significant category of chemical pollutants of aquatic ecosystems [2], and they pose a severe aesthetic and an ecological problem [3]. Even some of them are extremely toxic, carcinogenic, and mutagenic [4]. Various conventional wastewater treatment methods have been developed in the past decades for degradation and removal of dye from wastewaters, including ion exchange, reverse osmosis, flocculation, oxidation, coagulation, photochemical degradation, electrolysis, and activated sludge process [5, 6]. Among all methods, adsorption has been commonly used for wastewater treatment because the process is simple and cost-effective [7].

The use of nanomaterials provides ample opportunities to treat contaminated waters because of their properties like strong adsorption, low cost, enhanced photo-catalytic, and redox properties [8]. They have been used for the effective elimination of pollutants from the wastewater [9], which includes inorganic ions [10], organic pollutants [11], bacteria [12], and toxic metals [13]. Copper oxide nanoparticles (CuONPs) are among the most explored noble metals as they display excellent catalytic properties [14] and they possess similar properties to that of other metallic nanoparticles [15]. They have replaced silver, gold and platinum nanoparticles in wastewater treatment because of their lower cost [16, 17]. Copper oxide is a semi-conductive material with different magnetic, optical, and electrical properties [18], and its synthesis has gained much interest because of its numerous applications [19].

✉ Somaiah Sundarapandian
smspandian65@gmail.com

[1] Department of Ecology and Environmental Sciences, Pondicherry University, Puducherry 605014, India

Several methods for synthesizing CuONPs have been developed, which include the electrochemical route [20], polyethylene-glycol-dependent processes [21], sonochemical methods [22], sol–gel methods [23], etc. These methods yield low produce, are expensive, and are more laborious [17]. Additionally, these methods require high temperature and pressure [24]. The stabilizers used for nanoparticles in these methods are hazardous and toxic chemicals, and hence they pose a threat to the environment [25]. Henceforth, the present study focused on the green chemistry principles and demonstrated an eco-friendly approach for the synthesis of CuONPs using an aqueous leaf extract of *Wedelia urticifolia* and their use as potential adsorbent for Rhodamine-b (RhB) dye from water. The RhB dye removal has gained too much of attention from past two decades as it has carcinogenic and non-biodegradable chromophores [26]. The aromatic and water soluble dye has several toxic effects on human beings which include skin and eye irritation [27], mutation and cancer [28], etc.

The *W. urticifolia* plantbelongs to the Asteraceae family and is an erect, weak and perennial herb with elliptic leaves, bright yellow-colored flowers, terminal heads, and light camphor-like odour. It grows in many districts of China and East Asia. It has been used to treat fractures, muscle injuries, and infected wounds [29]. The plant is abundantly available within the university campus, where the present study was conducted. The use of plant leaf extract is favored over other green reducing agents in the present study because preparing leaf extract is simple, easy, cost-effective, and time-efficient. Additionally, the plant extracts contain both reducing as well as stabilizing biomolecules [30]. The pruning of overgrown stems and branches of *W. urticifolia* is done twice a year for encouraging its growth, and hence the plant waste generated (bio-waste) can be stored, dried, powdered, and used for preparing extract for the synthesis of nanoparticles at a larger scale. The secondary metabolites present in the plant extracts possess the property to reduce the metal ions [31, 32], and hence these extracts are used mostly for various nanoparticle synthesis [33].

Experimental Section

Chemicals and Materials

Anhydrous copper sulfate (analytical grade of purity $\geq$ 95%) was purchased from HiMedia Pvt. Ltd and Rhodamine-b (RhB) dye was purchased from Sigma Aldrich, India. Double distilled water was used for the preparation of extract and the solutions of metal salt.

Preparation of Leaf Extract

The fresh and healthy leaves of the *Wedelia urticifolia* plant were collected locally. Ten grams of fresh leaves were added to 100 ml of distilled water in 250 ml beaker and heated at 60 °C for 30 min. The leaf debris was separated from pale yellow extract formed by centrifugation at 10,000 rpm for 10 min, and the fresh supernatant obtained was used for nanoparticle synthesis.

Description of Biosynthesis Protocol

The copper oxide nanoparticles (CuONPs) were synthesized by adding the prepared leaf extract to 1 mM concentrated anhydrous copper sulfate solution in a ratio of 1:9. The mixture was continuously stirred at room temperature for 2 h. The brown color was formed in the solution, which indicates the synthesis of CuONPs. The colloidal obtained was centrifuged at 10,000 rpm for 10 min after 24 h of incubation time to obtain pellet, which was purified by washing three to five times with double distilled water. The purified nanoparticle pellet was dried in a hot air oven at 60 °C overnight for complete moisture evaporation. The final residue obtained was calcinated in a muffle furnace at 400 °C to remove the attached organic matter of plant, powdered and stored for further use.

Characterization of As-Synthesized Nanoparticles

The bioreduction of copper ions to CuONPs was initially confirmed by visual color change. For determining the structure of as-synthesized nanoparticles, the dried powder was scanned under XRD (PANalytical X'pert Pro) of scattering angle (2θ) between 20° to 80°. For FT-IR analysis (Thermo Nicolet, Model 6700), the centrifuged nanoparticle pellet was dried and mixed with KBr and examined in a range of 400 to 4000 cm^{-1}. The biomolecules responsible for reducing, capping, and stabilizing the as-synthesized nanoparticles were determined from this spectrum. For shape and morphology analysis, a fresh nano-colloid solution obtained was viewed under HRTEM (FEI, USA, Model Tecnai G2 F30-STWIN).

Adsorption Studies

To assess the dye adsorption ability, batch sorption experiments were conducted. The effect of adsorbent dosage (10 mg to 40 mg), initial dye concentration (10 ppm to 25 ppm), and contact time (30 min to 6 h) was investigated. Each variable was tested individually, keeping all other variables fixed. First, the known concentrations of as-synthesized CuONPs were added to 10 ml of dye solution and stirred using a magnetic stirrer at 120 rpm

at room temperature to mix the nanoparticle powder thoroughly. The samples were then withdrawn at different fixed time intervals of time, centrifuged at 10,000 rpm for 15 min, and the concentration of RhB dye present in the sample was measured. The following equation calculated the RhB removal:

$$Percentage\ of\ dye\ removal\ = \frac{Ci - Cf}{Ci} \times 100$$

where C_i is the initial concentration, and C_f is the final concentration of dye present in the solution. The initial and final concentrations of dye were measured before and after the adsorption process, respectively.

The total amount of RhB dye adsorbed (Q_t) per gram of CuONPs mass (M) at time t was calculated by:

$$Qt = \mathrm{V}\frac{(Ci - Cf)}{M}$$

V is the volume of the dye solution used.

Adsorption Isotherm

To understand the relationship between the adsorbent and the adsorbate at a constant temperature, studies on the adsorption isotherm are useful. In the present study, the adsorption data was fitted to Freundlich and Langmuir isotherm models, and the correlation coefficient (R^2) was calculated for both of them. The Freundlich isotherm model equation is represented as:

$$\ln Q_e = \ln K_F + 1/n \ln C_e$$

And the Langmuir isotherm model equation is represented as:

$$C_e/Q_e = 1/K_L Q_m + C_e/Q_m$$

where C_e (mg/L) is the dye concentration at equilibrium, Q_e (mg/g) is the equilibrium adsorption capacity, Q_m (mg/g) is the maximum adsorption capacity, and K_F and K_L (L/mg) are the Freundlich and Langmuir constants respectively.

The adsorption rate constant values were determined from the plot of $\ln(C_e)$ vs. $\ln(q_e)$ for the Freundlich isotherm model and $1/C_e$ vs. $1/Q_e$ for Langmuir isotherm model.

Adsorption Kinetics

Pseudo-first-order and pseud-second-order kinetic models were used to check the rate of adsorption of RhB dye in the present study and understand the mechanism of adsorption on the as-synthesized CuONPs. The pseudo-first-order kinetic equation is generally presented in the form:

$$\ln (Q_e - Q_t) = \ln Q_e - k_1 t$$

where q_e is the amounts of dye adsorbed (mg/g) at equilibrium, q_t is the dye amount adsorbed at time t and k_1 is the constant of adsorption rate.

And the pseudo-second-order adsorption kinetic model is expressed as:

$$t/Q_t = 1/k_2 Q_e^2 + t/Q_e$$

where k_2 is the adsorption rate constant.

The adsorption rate constant values are determined from the plot of $\ln(Q_e\text{-}Q_t)$ vs. t for the pseudo-first-order kinetic model and t/qt vs. t for the pseudo-second-order kinetic model.

Results and Discussion

Nanoparticle Synthesis

The reduction of copper ions to copper oxide nanoparticles (CuONPs) by *W. urticifolia* leaf extract was visually evident from the color change obtained. On adding the prepared leaf broth to 1 mM copper sulfate solution, the brown color was obtained in 2 h, which intensified with increase in contact time. In contrast, the color of controls, i.e., pale yellow in leaf broth and light blue in $CuSO_4$ solution prepared in distilled water, remained unchanged for the same time. It has been proposed that the color change in copper ions solution when mixed with plant extract is due to the formation of copper nanoparticles [34]. The color change in the solution mixture compared to the control solution indicates the nanoparticle formation [30, 31].

Characterization

UV–Visible (UV–Vis) Spectroscopy

The UV–Vis spectrum of CuONPs colloidal solutions was taken in the range of 200–800 nm, and the surface plosmon resonance peak was obtained at 280 nm (Fig. 1). The absorption band peak between 250 to 350 nm due to SPR excitation is designated to the copper oxide nanoparticle formation [35]. The result was well supported by the study conducted by Singh et al., who obtained a strong resonance peak in biologically synthesized CuONPs at 285 nm [36].

Dynamic Laser Spectroscopy (DLS)

The DLS spectrum revealed the average hydrodynamic size of 72.30 nm for as-synthesized CuONPs (Fig. 2).

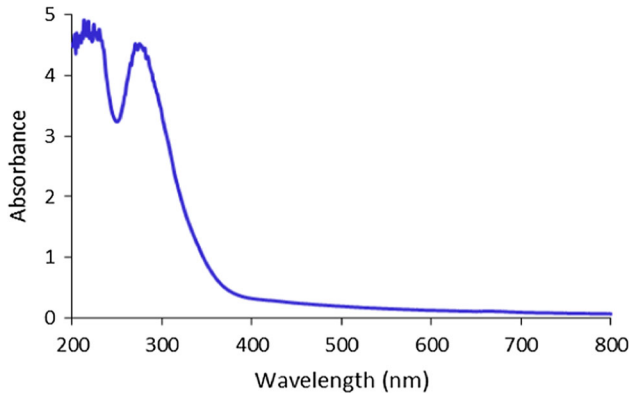

Fig. 1 The UV–Vis absorption spectra of copper oxide nano-colloid after 2 h of reaction time

Table 1 Peak indexing and calculated size of as-synthesized copper oxide nanoparticles from XRD

2θ (°)	hkl	FWHM (β) (radians)	Particle size (D nm)
35.64	(1 1 1)	0.0022	65.71
38.84	(2 0 0)	0.0023	63.69
48.78	(− 2 0 2)	0.0026	59.40
53.58	(0 2 0)	0.0036	43.23
58.32	(2 0 2)	0.0034	46.37
61.74	(− 1 1 3)	0.0026	60.75
66.30	(3 1 0)	0.0065	25.05
68.00	(2 2 0)	0.0044	37.48
72.6	(3 1 1)	0.0040	42.51
75.13	(− 2 2 2)	0.0056	30.80

X-Ray Diffraction (XRD)

The XRD peaks in as-synthesized CuONPs were observed at 2θ of 35.64, 38.84, 48.78, 53.58, 58.32, 61.74, 66.30, 68.00, 72.6, and 75.13 (Fig. 3). The peaks correspond to (1 1 1), (2 0 0), (-2 0 2), (0 2 0), (2 0 2), (-1 1 3), (3 1 0), (2 2 0), (3 1 1), and (-2 2 2) planes of copper oxide respectively when compared with standard ICSD Files (PDF Card No.: Cu-01–080-1916). The sharpness of the peaks in XRD spectrum reveals their crystalline structure [37]. Mehr and others obtained (1 1 1), (-2 0 2), (0 2 0), (2 0 2), (-1 1 3), (2 2 0) and (3 1 1) diffraction planes in XRD patterns of plant extract based synthesized CuONPs which are in well agreement with results of present study [38].

The average size of CuONPs was calculated using Debye–Scherrer formulae [8] from the width of the peaks in the XRD spectrum. The calculated size and peak indexing are presented in Table 1.

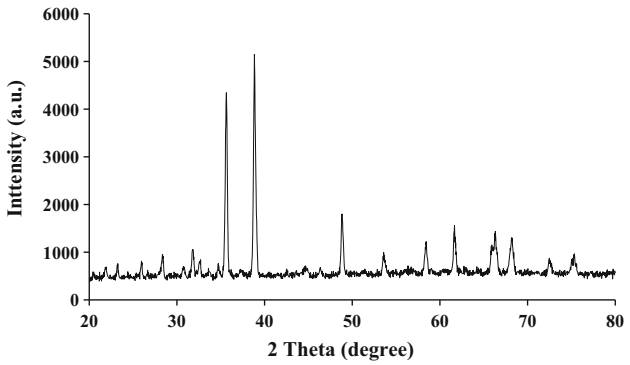

Fig. 3 The XRD pattern of copper oxide nanoparticles synthesized using *W. urticfolia* leaf extract

Fourier Transform Infrared Spectroscopy (FT-IR)

The FT-IR spectrum of leaf extract and as-synthesized CuONPs displayed several adsorption peaks that reflect the range of biomolecules (Fig. 4). FT-IR spectra of as-synthesized CuONPs depicted a spectral peak at 3442.2 cm^{-1},

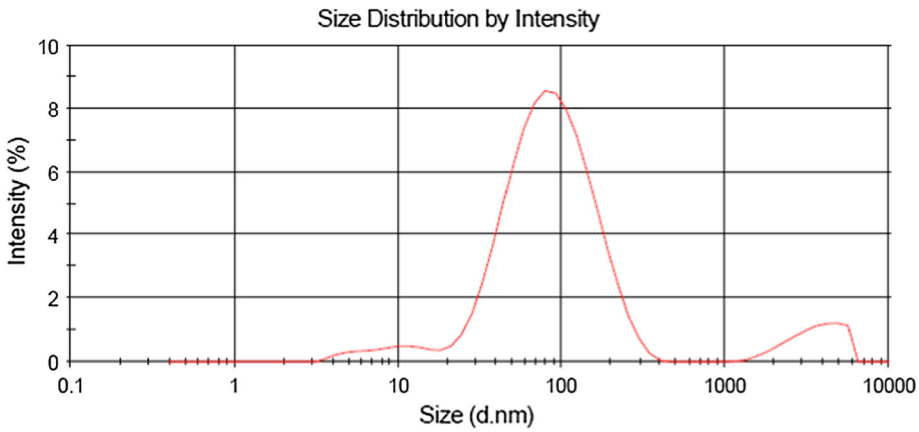

Fig. 2 The DLS spectrum depicting the average hydrodynamic size of as-synthesized copper oxide nano-colloid after 2 h of reaction time

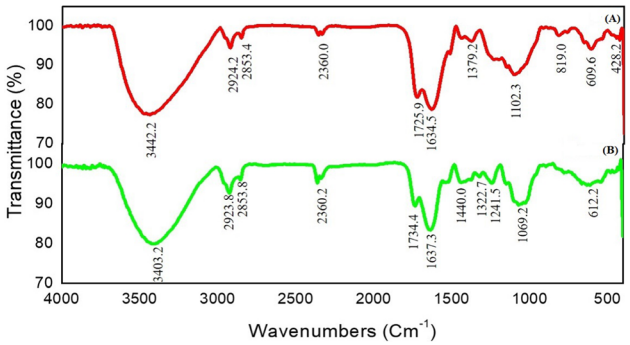

Fig. 4 FT-IR spectrum of as-synthesized copper oxide nanoparticles (**a**) and *Wedelia urticifolia* leaf extract (**b**)

due to a surface hydroxyl group (O–H) stretching. Two peaks at 2924.2 cm^{-1} and 2853.4 cm^{-1} are due to symmetric and asymmetric $–CH_2$ molecular stretching of alkenes. Peak found at 2360 cm^{-1} is due to strong O=C=O stretching of CO_2, 1725.9 cm^{-1}, and 1634.5 cm^{-1} are assigned to C = O stretching vibrations of α and β-unsaturated esters. The peak at 1379.2 cm^{-1} belongs to the C = C carboxylic group in polyphenols, 1102.3 cm^{-1}, and 819.0 cm^{-1} to C-O stretching of a secondary alcohol and 609.6 cm^{-1} to C-H stretching of alkyl halide. The peak at 428 cm^{-1} has been attributed to the Cu–O bond because the 400-600 cm^{-1} region in the FT-IR spectrum is assigned to M–O bonds (metal–oxygen bonds) [38]. Vishveshvar and others also obtained a peak at 488 cm^{-1} in the FT-IR spectrum of leaf extract synthesized CuONPs nanoparticles and assigned it to Cu–O bond vibrational frequencies [39]. Earlier, the peak for the metal–oxygen bond at 428 cm^{-1} was assigned to the formation of biosynthesized CuONPs as well [40]. There is a shift in peak position and peak intensity of biomolecules in as-synthesized CuONPs compared with the FT-IR spectrum of leaf extract due to their binding with nanoparticle surface [41].

Transmission Electron Microscopy (TEM)

The TEM images revealed the spherical shaped CuONPs of size less than 40 nm (Fig. 5). They also revealed that the nanoparticles were poly-dispersed and concentrated at a single place. The slight agglomeration in the as-synthesized nanoparticles could be due to the biological components used in the synthesis process. The agglomeration occurs because of hydroxyl groups of various phenolic compounds that undergo intermolecular hydrogen bonding [42]. The particles being concentrated at single places signify their tendency to aggregate [39, 43]. The CuONPs synthesized from plant extracts with spherical shape were in conformity with the previous reports [44–46].

Mechanism of CuONPs Synthesis

Plant extracts possess a range of biomolecules, among whom few can be responsible for nanoparticle synthesis, and hence synthesizing nanoparticles by such extracts is a complex process. Even predicting the exact mechanism of the synthesis process is also challenging. It has been proposed earlier that the major functional groups responsible for the reduction and stabilization of nanoparticles are amine, carbonyl, hydroxyl, and methoxide, and these functional groups are present in plant metabolites like alkaloids, carbohydrates, flavonoids, phenols, and proteins [47]. The disappearance of peaks at 1241.5 cm^{-1}, 1322.7 cm^{-1}, and 1440 cm^{-1} in IR spectra of leaf extract and the appearance of a peak at 1379.2 in the IR spectra of as-synthesized CuONPs indicates the possible role of polyphenol groups in nanoparticles synthesis. The relative shifts in the intensity of the strong peaks around 3400 cm^{-1} and 1630–1740 cm^{-1} can be attributed to the involvement of hydroxyl (–OH) groups and amines in the reduction and stabilization process during synthesis. Hence, the -OH group is suggested as the primary functional group to reduce and stabilize the as-synthesized

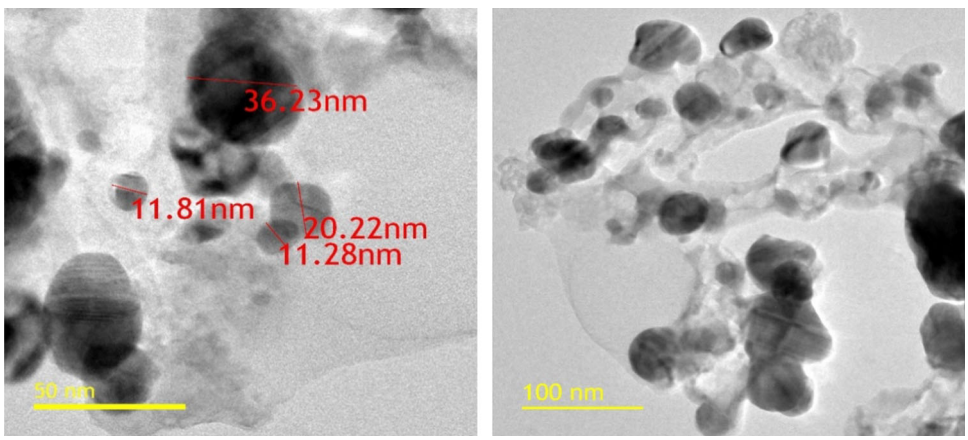

Fig. 5 TEM images of copper oxide nanoparticles synthesized using *W. urticfolia* leaf extract

nanoparticles in the present study. The CuONPs synthesis mechanism can be summarized as: the polyphenols present in the leaf extract of *W. urticifolia* bind with Cu^{2+} ions (which are formed after dissolving $CuSO_4$ in water) and form metal complexes which are then reduced to Cu^0 seed particles. The seed particles undergo aggregation, followed by nucleation. The graphical representation of the mechanism of CuONPs synthesis is presented in Fig. 6. Similar mechanisms for nanoparticle formation were proposed earlier [8, 46, 48]

Dye Adsorption

Adsorbent Dosage

The present study's data reveals that the adsorption of Rhodamine-b (RhB) dye molecules onto CuONPs was dose-dependent, and the percentage adsorption always increased with an increase in dosage (Fig. 7). This increased removal is because of more active available sites [49]. Such an increase in dye removal is attributed to the availability of more surface area [50]. It was proposed that the availability of more catalysts for attacking the dye's chromophoric system is responsible for an increase in dye removal [1].

Initial Dye Concentration

The percentage adsorption decreased on increasing the initial concentration of RhB dye in the solution in the present study (Fig. 8). The probable reason for the decrease in the percentage dye adsorption with an increase in initial concentration could be the saturation of adsorption sites at high dye concentrations. Sebeia and others also explained that the adsorption sites saturate because there are limited binding sites available on the adsorbent surface [51]. Suc

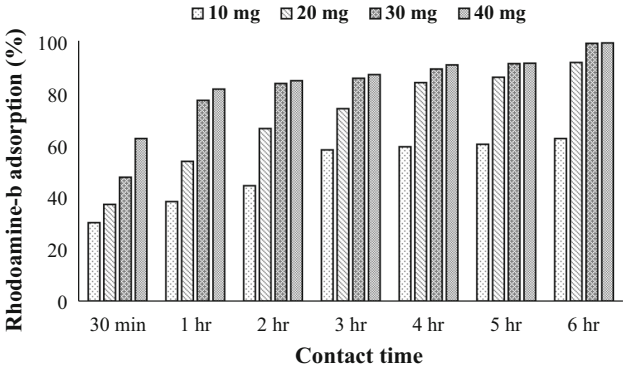

Fig. 7 The effect of as-synthesized copper oxide nanoparticle dosage on percentage rhodamine-b adsorption (RhB dye concentration = 25 ppm)

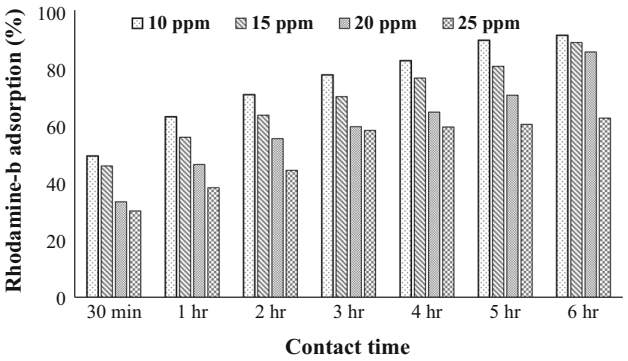

Fig. 8 The effect of initial rhodamine-b dye concentration on its percentage adsorption by as-synthesized copper oxide nanoparticles (CuONPs dosage = 10 mg/ 10 ml of dye solution)

and Chi, 2017 also observed a decrease in removal efficiency with an increase in initial dye concentration and explained that it is because of an increase in mass transfer resistance between the adsorbent and adsorbate, which results in the reduction of the rate of adsorption [52].

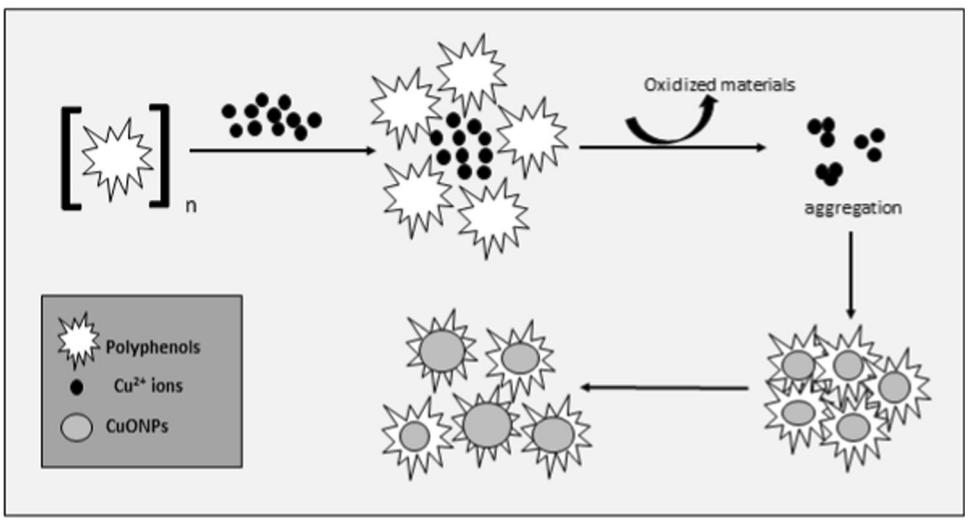

Fig. 6 Possible mechanism for CuONPs synthesis by *Wedelia urticifolia* leaf extract

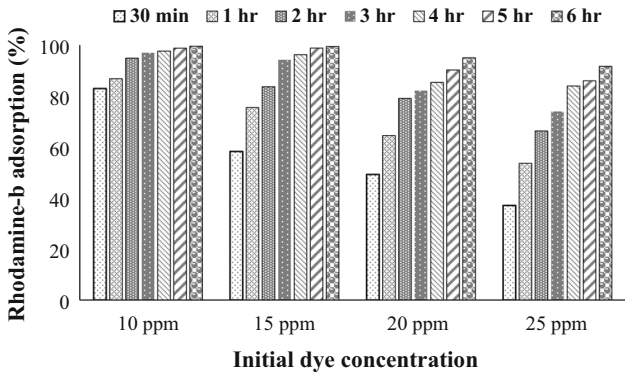

Fig. 9 The effect of contact time on adsorption of rhodamine-b dye by as-synthesized copper oxide nanoparticles (CuONPs dosage = 20 mg)

Contact Time

The percentage of dye adsorption also increases with an increase in the contact time (Fig. 9). Asl et al. [53] and Kale and Kane [54] also found that the decolorization increased with the contact time when nanoparticle concentration was kept the same. According to them, more contact time signifies that more time is given for the reaction. The rate of Coomassie brilliant blue decolorization also increased when the incubation time of CuONPs was increased [37].

The results displayed a two-step adsorption process. In the beginning, it was fast, and later it reduced with time, and the probable reason could be the availability of all active adsorbing sites at the beginning, which get reduced with time as adsorption takes place [52]. Sebeia and others [51] also found that the sorption rate of dye is fast in the beginning, and it gets slowed down with the time and attributed it to the availability of more adsorption sites in the beginning. The number of available sites was found decreasing with the time earlier by Kim and others [55].

Adsorption Isotherm

The Freundlich and Langmuir isotherm models were employed in the present study to describe the behavior of RhB dye adsorption in the presence of as-synthesized CuONPs, and the fitting curves are presented in Fig. 10a and b respectively. The R^2 values obtained at 20 mg of CuONPs dosage per 10 ml of different RhB dye solutions were 0.97 and 0.89 for Freundlich isotherm and Langmuir models. The higher R^2 value of the Freundlich isotherm model suggests that adsorption in the present study is a monolayer and heterogeneous process [56].

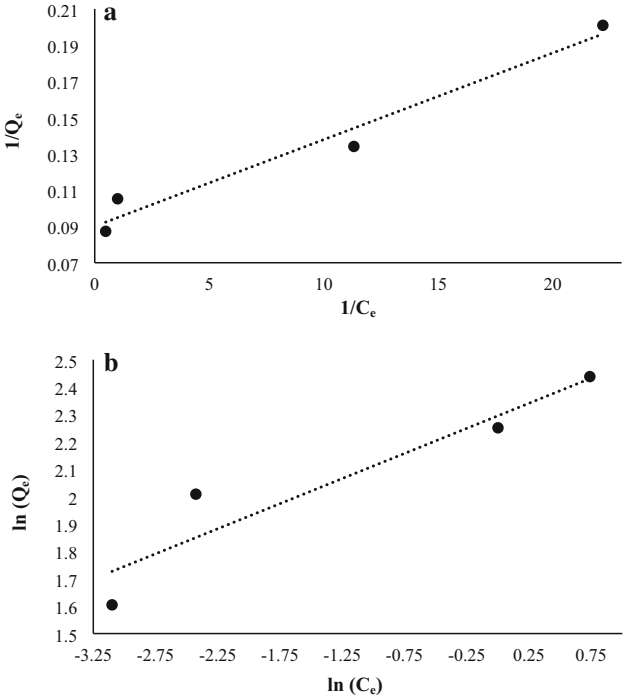

Fig. 10 Freundlich isotherm (**a**) and Langmuir isotherm (**b**) plots for rhodamine-b dye adsorption on as-synthesized copper oxide nanoparticles

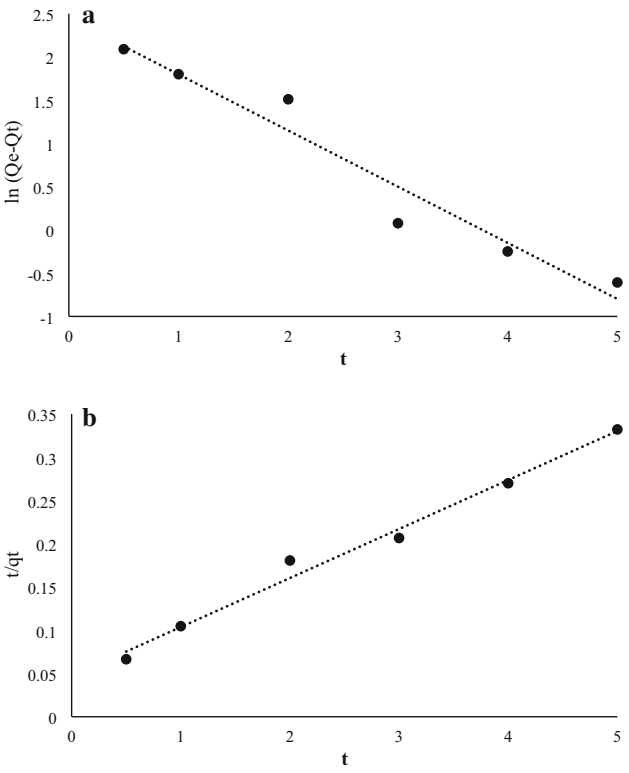

Fig. 11 Linearization of the data through (**a**) pseudo-first-order kinetic model and (**b**) pseudo-second-order kinetic model

Adsorption Kinetics

The fitting curves of pseudo-first-order and pseudo-second-order kinetic models are presented in Fig. 11a and b, respectively, for 25 ppm concentrated RhB dye. The higher R^2 value of the pseudo-second-order model (0.99) compared to the pseudo-first-order kinetic model (0.95) suggested that it describes the process of RhB adsorption on as-synthesized CuONPs better than the pseudo-first-order kinetic model [57]. The adsorption rate constant calculated based on the pseudo-second-order kinetic model is 0.0566 g/mg min^{-1}.

Additionally, the synthesized nanoparticles does not show any kind of aggregation after dye adsorption process as observed in SEM image (Fig. 12), hence, it is perceived that these nanoparticles can be recycled and reused for repeated adsorption.

Conclusion

The present study substantiates the use of *W. urticifolia* leaf extract as a green, reducing agent for the successful synthesis of copper oxide nanoparticles at a larger scale. The synthesis process adopted is straightforward, cost-effective, non-toxic, and pollution-free. The vital concern about nanoparticles is their stability, and various polymers or surfactants are used for stabilizing the nanoparticles, but, in the present study, copper oxide nanoparticles were stabilized by capping agents present within the plant leaf extract which is an advantage in conducted study. Various characterization techniques confirmed their nano properties. Additionally, the as-synthesized nanoparticles were used for dye adsorption because complete removal of dyes from wastewater is essential for water pollution minimization. The dye adsorption was observed to be increasing with increase in adsorbent dosage and contact time while it decreased with increase in the dye concentration. Over 99% of rhodamine-b dye adsorption was achieved in the present study (10 ppm concentrated dye) and the adsorption process fits well with Freundlich isotherm and pseudo-second-order kinetic model. Overall, the results revealed a significant adsorption capability for Rhodamine-b dye and hence, the study concludes that the synthesized copper oxide nanoparticles can be used as alternate adsorbents to available expensive wastewater treatment techniques. The proposed wastewater treatment method is recommended considering its complete green approach and good adsorption performance.

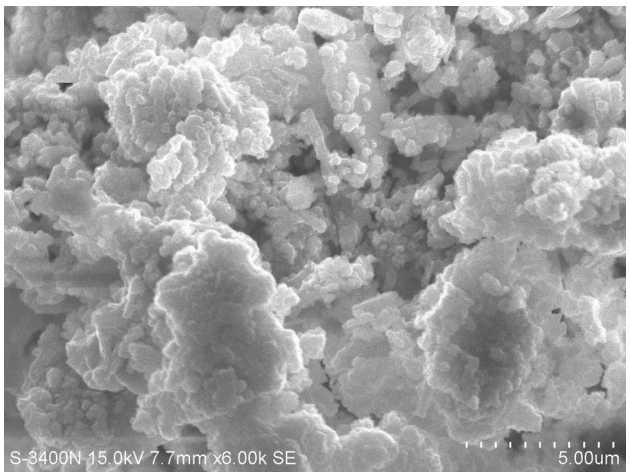

Fig. 12 SEM image of copper oxide nanoparticles after dye adsorption process

Acknowledgments The authors are grateful to the UGC for providing scholarship during the study period to MYR. The authors are thankful to Central Instrumentation Facility, Pondicherry University for Fourier transform infrared and Transmission electron microscopy analysis, and the Centre for Nanoscience and Nanotechnology for X-ray diffraction characterization. We acknowledge the help of Mr. Mannmohan, Ph.D. Scholar, Centre for Pollution Control and Environmental Engineering, Pondicherry University.

Funding This research did not receive any specific grant from funding agencies in the public, commercial, or not-for-profit sectors.

Compliance with Ethical Standards

Conflict of interest The authors declare that they have no conflict of interest.

References

1. Y. R. Zhang, P. Su, J. Huang, Q. R. Wang, and B. X. Zhao (2015). *Chem. Eng. J.* **262**, 313–318.
2. S. Khan and A. Malik (2018). *Environ. Sci. Pollut. Res.* **25**, 4446–4458.
3. F. Nekouei, S. Nekouei, I. Tyagi, and V. K. Gupta (2015). *J. Mol. Liq.* **201**, 124–133.
4. M. Sharma, P. Das, and S. Datta, *In Waste Valorisation and Recycling*. (Springer, Singapore, 2019), pp. 453–466.
5. S. Rajendran, M. M. Khan, F. Gracia, J. Qin, V. K. Gupta, and S. Arumainathan (2016). *Sci. Rep.* **6**, 31641.
6. S. N. Jain and P. R. Gogate (2019). *Int. J. Environ. Res.* **13**, 337–347.
7. S. K. R. Yadanaparthi, D. Graybill, and R. Von-Wandruszka (2009). *J. Hazard. Mater.* **171**, 1–15.
8. M. Y. Rather, and S. Sundarapandian, (2020). *Appl. Nanosci.* https://doi.org/https://doi.org/10.1007/s13204-020-01366-2.
9. M. Ghaedi, H. Z. Khafri, A. Asfaram, and A. Goudarzi (2016). *Spectrochim. Acta. Part A.* **152**, 233–240.
10. E. A. Deliyanni, N. K. Lazaridis, E. N. Peleka, and K. A. Matis (2004). *Environ. Sci. Pollut. Res.* **11**, 18–21.
11. J. Yan, L. Han, W. Gao, S. Xue, and M. Chen (2015). *Bioresour. Technol.* **175**, 269–274.
12. R. S. Kalhapure, S. J. Sonawane, D. R. Sikwal, M. Jadhav, S. Rambharose, C. Mocktar, and T. Govender (2015). *Colloids. Surf. B.* **136**, 651–658.

13. W. W. Tang, G. M. Zeng, J. L. Gong, J. Liang, P. Xu, C. Zhang, and B. B. Huang (2014). *Sci. Total Environ.* **468**, 1014–1027.
14. S. Raina, A. Roy, and N. Bharadvaja (2020). Environ. Nanotechnol. Monit. *Manage.* **13**, 100278.
15. N. Nagar and V. Devra (2018). *Mater. Chem. Phys.* **213**, 44–51.
16. J. A. Eastman, S. U. S. Choi, S. Li, W. Yu, and L. J. Thompson (2001). *Appl. Phys. Lett.* **78** (6), 718–720.
17. N. Nazar, I. Bibi, S. Kamal, M. Iqbal, S. Nouren, K. Jilani, M. Umair, and S. Ata (2018). *Int. J. Biol. Macromol.* **106**, 1203–1210.
18. Q. Zhang, K. Zhang, D. Xu, G. Yang, H. Huang, F. Nie, C. Liu, and S. Yang (2014). *Prog. Mater. Sci.* **60**, 208–337.
19. K. Saravanakumar, S. Shanmugam, N. B. Varukattu, D. MubarakAli, K. Kathiresan, and M. H. Wang (2019). *J. Photochem. Photobiol. B.*. **190**, 103–109.
20. A. A. Keller, A. S. Adeleye, J. R. Conway, K. L. Garner, L. Zhao, G. N. Cherr, J. Hong, J. L. Gardea-Torresdey, H. A. Godwin, S. Hanna, and Z. Ji (2017). *NanoImpact.* **7**, 28–40.
21. C. C. Vidyasagar, Y. A. Naik, T. G. Venkatesha, and R. Viswanatha (2012). *NanoMicro. Lett.* **4**, 73–77.
22. I. Perelshtein, A. Lipovsky, N. Perkas, T. Tzanov, and A. Gedanken (2016). *Beilstein. J. Nanotechnol.* **7**, 1–8.
23. J. Jayaprakash, N. Srinivasan, P. Chandrasekaran, and E. K. Girija (2015). *Spectrochim. Acta. Part. A.* **136**, 1803–1806.
24. S. R. Ali, M. R. Ghadimi, M. Fecioru-Morariu, B. Beschoten, and G. Güntherodt (2012). *Phys. Rev. B.*. **85**, 012404.
25. M. Asif (2015). *Chem. Int.* **1**, 134–163.
26. M. Onditi, G. Bosire, E. Changamu, and C. Ngila (2019). *Starch.* **71** (1800127), 1–8.
27. S. Francis, S. Joseph, E. P. Koshy, and B. Mathew (2017). *Environ. Sci. Pollut. Res.* **24**, 17347–17357.
28. S. Singh, A. Kumar, and H. (2020). *Appl. Water Sci.* **10,** 185 (2020).
29. L. Zhu, Y. J. Tian, Y. C. Yin, and S. M. Zhu, *Ital*. (J. Food, Sci, 2012), p. 24.
30. M. Y. Rather, M. Shincy, and S. Sundarapandian (2020). *Micros. Res. Techniq*. DOI: https://doi.org/10.1002/jemt.23499.
31. V. Kumar, R. K. Gundampati, D. K. Singh, M. V. Jagannadham, S. Sundar, and S. H. Hasan (2016). *J. Ind. Eng. Chem.* **37**, 224–236.
32. Y. Choi, S. Kang, S. H. Cha, H. S. Kim, K. Song, Y. J. Lee, K. Kim, Y. S. Kim, S. Cho, and Y. Park (2018). *Nanoscale. Res. Lett.* **13**, 1–10.
33. P. Kuppusamy, M. M. Yusoff, G. P. Maniam, and N. Govindan (2016). Saudi. *Pharm. J.* **24**, 473–484.
34. H. J. Lee, G. Lee, N. R. Jang, J. H. Yun, J. Y. Song, and B. S. Kim (2011). *Nanotechnology.* **1**, 371–374.
35. D. Das, B. C. Nath, P. Phukon, and S. K. Dolui (2013). *Colloids Surf. B.* **101**, 430–433.
36. K. K. Singh, K. K. Senapati, and K. C. Sarma (2017). *J. Environ. Chem. Eng.* **5**, 2214–2221.
37. R. Sankar, P. Manikandan, V. Malarvizhi, T. Fathima, K. S. Shivashangari, and V. Ravikumar (2014). *Spectrochim. Acta. Part A.* **121**, 746–750.
38. E. S. Mehr, M. Sorbiun, A. Ramazani, and S. T. Fardood (2018). *J. Mater. Sci.-Mater. Electron.* **29**, 1333–1340.
39. K. Vishveshvar, M. A. Krishnan, K. Haribabu, and S. Vishnuprasad (2018). *BioNanoScience.* **8**, 554–558.
40. F. D. Koca, D. Demirezen-Yilmaz, F. Duman, and I. Ocsoy (2018). *Chem. Ecol.* **34**, 839–853.
41. R. Majumdar, B. G. Bag, and N. Maity (2013). *Int. Nano. Lett.* **3**, 53.
42. A. Munin and F. Edwards-Lévy (2011). *Pharmaceutics.* **3**, 793–829.
43. S. Dagher, Y. Haik, A. I. Ayesh, and N. Tit (2014). *J. Lumin.* **151**, 149–154.
44. S. Gunalan, R. Sivaraj, and R. Venckatesh (2012). *Spectrochim. Acta. Part. A.* **97**, 1140–1144.
45. M. Nasrollahzadeh, M. Maham, and S. M. Sajadi (2015). *J. Colloid. Interface. Sci.* **455**, 245–253.
46. A. H. Keihan, H. Veisi, and H. Veasi (2017). *Appl. Organomet. Chem.* **31**, 3642.
47. G. K. Devi, K. S. Kumar, R. Parthiban, and K. Kalishwaralal (2017). *Microb. Pathog.* **102**, 120–132.
48. N. Edayadulla, N. Basavegowda, and Y. R. Lee (2015). *J. Ind. Eng. Chem.* **21**, 1365–1372.
49. P. Zhang, D. O'Connor, Y. Wang, L. Jiang, T. Xia, L. Wang, D. C. Tsang, Y. S. Ok, and D. Hou (2020). *J. Hazard. Mater.* **384**, 121286.
50. K. K. Deepa, M. Sathishkumar, A. R. Binupriya, G. S. Murugesan, K. Swaminathan, and S. E. Yun (2006). *Chemosphere.* **62**, 833–840.
51. N. Sebeia, M. Jabli, A. Ghith, and T. A. Saleh (2020). *Arab. J. Chem.* **13**, 4263–4274.
52. N. V. Suc, and D. Kim Chi (2017). *J. Dispersion. Sci. Technol.* **38**, 216–222.
53. M. N. Asl, N. M. Mahmodi, P. Teymouri, B. Shahmoradi, R. Rezaee, and A. Maleki (2016). *Desalin. Water. Treat.* **57**, 25278–25287.
54. R. D. Kale and P. B. Kane (2019). Groundw. *Sustain. Dev.* **8**, 309–318.
55. T. S. Kim, H. J. Song, M. A. Dar, H. J. Lee, and D. W. Kim (2018). *Appl. Surf. Sci.* **439**, 364–370.
56. S. Sharma, A. Hasan, N. Kumar, and L. M. Pandey (2018). *Environ. Sci. Pollut. Res.* **25**, 21605–21615.
57. A. U. Rajapaksha, S. S. Chen, D. C. Tsang, M. Zhang, M. Vithanage, S. Mandal, B. Gao, N. S. Bolan, and Y. S. Ok (2016). *Chemosphere.* **148**, 276–291.